Chemical Science International Journal

19(4): 1-12, 2017; Article no.CSIJ.34082
ISSN: 2456-706X
(Past name: American Chemical Science Journal, Past ISSN: 2249-0205)

Effective Microporosity for Enhanced Adsorption Capacity of Cr (VI) from Dilute Aqueous Solution: Isotherm and Kinetics

Lloyd Mukosha[1,2*], Maurice S. Onyango[1], Aoyi Ochieng[3] and John Siame[2]

[1]Department of Chemical, Metallurgical and Materials Engineering, Tshwane University of Technology, Pretoria, Private Bag X680, South Africa.
[2]Department of Chemical Engineering, Copperbelt University, Kitwe, P.O.Box 21692, Zambia.
[3]Department of Chemical Engineering, Vaal University of Technology, Vanderbijlpark 1900, South Africa.

Authors' contributions

This work was carried out in collaboration between all authors. Authors MSO and AO designed the study, organized experiment requisites and interpretation of results. Authors LM and JS conducted experiments, managed literature searches and analyzed samples and results. Author LM wrote the first draft of the manuscript. All authors read and approved the final manuscript.

Article Information

DOI: 10.9734/CSJI/2017/34082
Editor(s):
(1) Nagatoshi Nishiwaki, Kochi University of Technology, Japan.
(2) T. P. West, Department of Chemistry, Texas A&M University-Commerce, USA.
Reviewers:
(1) Farid I. El-Dossoki, Port-Said University, Egypt.
(2) Jelena Kiurski, University Business Academy, Novi Sad, Serbia.
(3) Saima Fazal, South China University of Technology, China.
Complete Peer review History: http://www.sciencedomain.org/review-history/19612

Original Research Article

Received 12th May 2017
Accepted 13th June 2017
Published 19th June 2017

ABSTRACT

The adsorbent pore structure significant to enhanced adsorption capacity of Cr (VI) from dilute aqueous solution is evaluated. As reference, low-cost micro-mesoporous activated carbon (AC) of high basicity, mesoporosity centred about 2.4 nm, and effective microporosity centred about 0.9 nm was tested for removal of Cr (VI) from dilute aqueous solution in batch mode. At pH 2 the low-cost AC exhibited highly improved Langmuir Cr (VI) capacity of 115 mg/g which was competitive to high performance commercial AC. A Comparison with treated characterization results of literature adsorbents/ACs showed that moderate to high effective micropore volume of average pore-size

**Corresponding author: E-mail: loimwimba@yahoo.com;*

about 0.9 ± 0.1 nm is critical for increased adsorption capacity of Cr (VI) from dilute aqueous solutions. The mesostructure of the tested low-cost AC was associated with rapid kinetics that was fitted by the Pseudo-second kinetics model. While Biot numbers suggested slight significant contribution of intraparticle diffusion. It is hoped that this study may be a useful contribution to development of effective adsorbents for the efficient abatement of toxic Cr (VI) from wastewater and water.

Keywords: Cr (VI) adsorption; dilute solution; adsorbent properties; micro-mesoporous; effective microporosity.

1. INTRODUCTION

The necessity for removal of highly toxic Cr (VI) from wastewaters and the highly feasible use of the economical and efficient adsorption technology have been adequately discussed [1-3]. It is at low concentration of Cr (VI) in water bodies that is significant to environmental protection as reflected in stringent Cr (VI) contaminant limits of 0.05 mg/L in drinking water and 0.1 mg/L for wastewater discharge to surface waters [4]. For solution Cr (VI) concentration < 1000 mg/L, the predominant species are hydrogen chromate oxyanion ($HCrO_4^-$) in pH 1 – 6.5 and chromate oxyanion (CrO_4^{2-}) in pH 6.5 – 10 [2]. With reference to diameter of CrO_4^{2-} of ca. ≈ 0.50 nm [5] and its spatial arrangement, it could be assumed that the diameter of $HCrO_4^-$ (a product of protonation reaction: $CrO_4^{2-} + H^+ \leftrightarrow HCrO_4^-$) would be similar at about 0.50 nm. Literature studies on the adsorption of Cr (VI) in solution pH 2 - 5 has showed that adsorbent specific surface functionality (acidic or basic) would enhance affinity for $HCrO_4^-$ either by ion-exchange interaction [6] or electrostatic attraction [7,8]. It is evident from X-ray Photoelectron Spectroscopy analysis that $HCrO_4^-$/biosorbent interaction could plausibly proceed through adsorption-coupled reduction and chemisorption or complexation of resultant Cr^{3+} dependent on amount of acidic surface groups [8-10].

At present, however, the outstanding fact about Cr (VI) adsorption is the lack of conclusive empirical evidence on the relevant pore-size distribution (PSD) for enhanced adsorption capacity from dilute industrial wastewaters [typically < 400 ppm] significant to environmental protection. Referenced to silica nanoparticles of mean adsorption pore size about 7.0 nm, the researchers [11] concluded that adsorbent broad PSD, not surface area or average pore size, is important for enhanced removal of Cr (VI) from wastewater. In another study [12], ordered mesoporous carbon (OMC) of PSD centered about 22 nm was reported to have very high capacity for Cr (VI) than micro-mesoporous activated carbon (AC) of wide PSD centered about 3.2 nm. Contrary to above both reports, it is known that the adsorption process would follow a sequential occupancy of adsorption sites based on level of adsorption potential [13-15]. In this sense, for adsorption from dilute solutions, the adsorption potential would be highest in effective micropores with monolayer or primary volume filling capacity due to strong overlapping of adsorption potential from opposite walls, as opposed to surface coverage in wider pores. This means that enhancement of adsorption potential in effective micropores depends on the ratio of micropore size to adsorbate size. In related study, the high butane adsorption capacity from dilute solution was reported to occur in effective micropores with primary volume filling [16]. This should be contrasted with adsorption from concentrated solutions when capacity could be a function of total micropore volume.

The contribution of knowledge of the relevant PSD for enhanced Cr (VI) capacity from dilute solutions would be significant for optimal design of future adsorbents. Interestingly, many studies have explored the potential application of abundantly available biomass wastes for development of low-cost adsorbents/ACs for abatement of Cr (VI) from wastewater [1,2,17]. The low-cost adsorbents/ACs were developed using the backward approach of first developing the adsorbent and then testing for quality in adsorption of Cr (VI). However, most of developed low-cost adsorbents/ACs have showed low Cr (VI) capacities from dilute aqueous solutions. In practical application, low Cr (VI) capacities on low-cost adsorbents would translate into usage of large quantities of adsorbent and design of large sized adsorption units. The handling and disposal of large quantities of spent adsorbent could also be an environmental problem. Therefore, there is still need to develop new low-cost adsorbents of high efficient removal of Cr (VI) from dilute aqueous solutions.

In this study, attempt is made to evaluate the effective microporosity for enhanced Cr (VI) capacity from dilute aqueous solution and, thereby, promote the forward approach of incorporating relevant adsorbent properties at development stage. Low-cost sawdust AC (denoted L-AC) developed at our previously determined optimum conditions [16] was submitted for removal of Cr (VI) from dilute aqueous media. The L-AC was characterized for relevant adsorptive properties and batch adsorption studies to evaluate effect of pH, equilibrium capacity and kinetics were conducted. Importantly, the pore structure the L-AC is discussed in relation to adsorption potentials for Cr (VI) from dilute aqueous media. The equilibrium capacity was compared with commercial AC. Thereafter, using our L-AC as reference, literature adsorbent/AC characterization results were treated and their relevance to results of comparative analysis was made to validate the effective micropore average size available for adsorption for enhanced Cr (VI) capacity from dilute solutions.

2. EXPERIMENTATION

2.1 Materials

The low-cost AC (L-AC) was developed from Pine tree (*Pinus patula*) sawdust obtained locally (Singisi Sawmill, KwaZulu Natal, South Africa). The commercial AC (Norit RO 0.8), vendor specified as suitable for wastewater treatment was purchased from Sigma, USA and used for comparison. Potassium dichromate ($K_2Cr_2O_7$, 99+ %) powder was purchased from Sigma, USA. Hydrochloric acid (HCl, 32%) Sodium Chloride standard solution (NaCl, 99.5%) and Sodium Hydroxide pellets (NaOH, ≥ 95%) were purchased from SMM, South Africa. Stock solutions were prepared using deionised water. All chemicals used were of analytical reagent grade.

2.2 Development and Characterization of Activated Carbon

The carbonization and activation of carbon samples were performed in a stainless steel vertical fixed-bed tubular reactor. Equipments and details of preliminary optimization of carbonization/activation processes have been previously reported [18]. Briefly, the *P. patula* sawdust was carbonized in continuous N_2 flow (570 mL/min) at 10 K/min to 800°C and 2 hrs, and the char cooled to ambient temperature in N_2 flow. To develop L-AC, the prepared char was heated in continuous preheated N_2 flow (180°C, 570 mL/min) at 10 K/min to 800°C and superheated steam (180°C, 1.6 bar, and 780 mL/min) activated for 1.5 hrs, and cooled to ambient temperature in N_2 flow and stored in a desiccator. The during activation or in-situ modification of surface groups occurred at the activation temperature in flowing N_2-steam mixture.

The outgassed L-AC sample was analyzed for textural properties using 77K N_2-adsorption (TriStar II 2030, Micromeritics) and 273K CO_2-adsorption (ASAP 2020, Micromeritics), and surface morphology using scanning electron microscope (SEM, Cambridge Instrument 360). While the total acidity and basicity were determined by the standardized Boehm titration method and the pH point of zero charge (pH_{PZC}) from proton binding isotherm obtained by the manual potentiometric titration method. Details of instruments and procedures were previously reported [16]. The bulk density was determined using the graduated cylinder method. The average pore size (L_{AVE}, nm) of micropores available for adsorption was calculated from the geometrical relation [19]:

$$L_{AVE} = 2 \times 10^3 V_{MIC}/S_{MIC} \quad (1)$$

where, V_{MIC} (cm^3/g) and S_{MIC} (m^2/g) are t-plot (analogue of α-plot [13]) micropore volume and surface area respectively.

2.3 Batch Equilibrium

Equilibrium adsorption studies were conducted in sample bottles with 0.8 g/L-AC in solutions of known Cr (VI) concentrations shaken in a thermostated water shaker (Labcom, Maraisburg) at 200 rpm and 25°C for 24 hrs equilibration, paper filtration and the filtrates Cr (VI) concentrations determined by the EPA recommended 1, 5-Diphenylcarbazide method using UV-Vis spectrophotometer (Libra S12, UK) at 543 nm. The effect of pH was studied using triplicate samples. Solutions pH was adjusted using HCl or NaOH solutions, and using pre-calibrated pH meter (Orion 4 star, USA). Subsequent to determining the adsorption optimum pH all other adsorption tests were carried out at that optimum pH. The uptake q_e (mg/g) and percentage removal φ (%) were calculated according to equations (2) and (3) respectively.

$$q_e = (C_O - C_e)V_S/m \quad (2)$$

$$\varphi = 100[(C_O - C_e)/C_O] \quad (3)$$

where, C_O is the solute initial concentration (mg/L), C_e is the equilibrium solute concentration in solution (mg/L), V_S is the solution volume (L), and m is mass of AC (g).

The isotherm parameters were evaluated using the isotherm models of the Langmuir (equation 4) and Freundlich (equation 5) [20]. The agreement of model to data was validated by nonlinear regression of minimizing the Chi-squared (χ2) function per equation 6 [20], with solutions generated using Microsoft Excel 2010, Add-in solver.

$$\frac{q_e}{Q_{max}} = \frac{K_L C_e}{1+K_L C_e} \quad (4)$$

$$q_e = K_F(C_e)^{Fr} \quad (5)$$

$$\chi^2 = \sum_{i=1}^{n} \frac{\left(q_{e(expt)i} - q_{e(calc)i}\right)^2}{q_{e(expt)i}} \quad (6)$$

where, Q_{max} is the monolayer adsorption capacity (mg/g), and K_L is the Langmuir constant (L/mg). K_F is Freundlich constant related to the adsorption capacity (mg/g) and Fr is the heterogeneous factor.

2.4 Batch Kinetics

Batch adsorption kinetics tests were conducted for the evaluation of the rate constants and diffusion parameters. A laboratory batch stirred tank with 600 mL solution of 50 mg/L Cr (VI) and stirring speed of 400 rpm was used by the method detailed in [21]. Syringe filters (0.2 µm) were used to withdraw 5 mL aliquot samples at predetermined time intervals. The variable studied was initial concentration. The uptake with time t (min), $q(t)$ (mg/g) was calculated by:

$$q(t) = \big(C_O - C(t)\big)V_S/m \quad (7)$$

where, $C(t)$ is solute concentration in (mg/L) at time, t.

The kinetics rate constants were evaluated using the adsorption surface reaction models of the pseudo first-order (equation 8) and the pseudo second-order (equation 9) [8,22], with conformity of model to data assessed through minimum Chi-squared function, equation 6. While the diffusion controlling stage was evaluated from the adsorption mass transfer Biot (Bi) number, equation 10 [23] with the batch film transfer coefficient (k_{fb}, cm/s) determined by the Mathews & Weber (M&W) linear driving force (LDF) rate law (equation 12) [24] and the effective intraparticle diffusion coefficient (D_{eff}, cm^2/s) approximated by the Patterson diffusion model (equations 13 – 17) [23].

$$q(t) = q_1(1 - e^{-k_1 t}) \quad (8)$$

$$q(t) = \frac{q_2 k_2 t}{1+q_2 k_2 t} = \frac{ht}{q_2+ht} \quad (9)$$

$$Bi = \frac{k_{fb} d_p C_O}{2D_{eff}\rho_p q_O} \quad (10)$$

$$\rho_p = \rho_b/(1 - \varepsilon_b) \quad (11)$$

$$ln\left[\frac{C(t)}{C_O}\right] = -\left[\frac{6k_{fb}m}{d_p\rho_p V_S}\right]t \quad (12)$$

$$U(t) = \frac{w+1}{w}\left\{\left(1 - \frac{1}{\theta-\beta}\right)\begin{bmatrix}\theta exp(\theta^2\tau)\left(1+erf\left(\theta\sqrt{\tau}\right)\right)\\ -\beta exp(\beta^2\tau)\left(1+erf\left(\beta\sqrt{\tau}\right)\right)\end{bmatrix}\right\} \quad (13)$$

$$U(t) = (C_O - C(t))/(C_O - C_e) \quad (14)$$

$$w = (C_O - C_e)/C_O \quad (15)$$

$$\tau = 4D_{eff}t/{d_p}^2 \quad (16)$$

$$x^2 + 3wx - 3w = 0 \quad (17)$$

where, q_1 and q_2 are adsorbed quantities (mg/g), k_1 and k_2 are rate constants, h is initial sorption rate (min), q_O adsorbed quantity (mg/g) in equilibrium with C_O, d_p is particle diameter (cm), ρ_p is particle density (g/cm^3) estimated by equation 11 [23], ρ_b is bulk density (g/cm^3), ε_b is bed porosity of typically about 0.4 for AC [25], $U(t)$ is the fractional attainment to equilibrium; w is the equilibrium partition ratio ($0 < w < 1$ indicates finite solution case i.e. concentration of adsorptive in solution continuously changes from initial to equilibrium, and $w > 1$ indicates infinite solution case i.e. concentration of adsorptive remains constant in solution), τ is dimensionless time constant and, the Θ and β terms are the negative and positive roots respectively, of equation (17).

3. RESULTS AND DISCUSSION

3.1 Activated Carbon Characterization

Fig. 1 shows the 77K N_2-adsorption/desorption isotherm curve of L-AC. The exhibited type IV

isotherm with H3-type hysteresis loop in the range P/P_O (0.4 – 0.8) was indicative of narrow distribution of relatively uniform or ordered mesopores. From SEM micrograph of Fig. 2, platelike particles with some slit-pores and dominant similar circular pores were observed. The high N_2 adsorption start point in Fig. 1 suggested N_2 molecule diffusional restrictions in narrow micropore (< 0.5 nm) at 77K and P/P_O < 0.06 in our short experiment time of 8 hrs [15] and, therefore, narrow microporosity was evaluated from CO_2-adsorption isotherm data at 273K and P/P_O < 0.04 and 8 hrs [insert in Fig. 1].

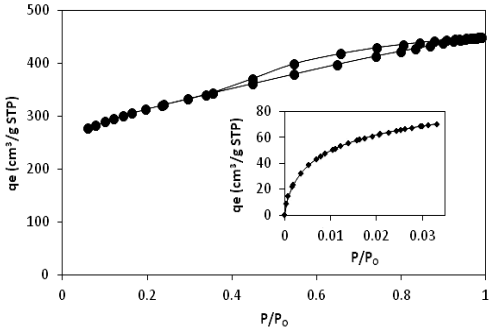

Fig. 1. 77K N_2- adsorption/desorption isotherms (●) of L-AC [Insert: 273K CO_2-adsorption isotherms (♦) of L-AC]

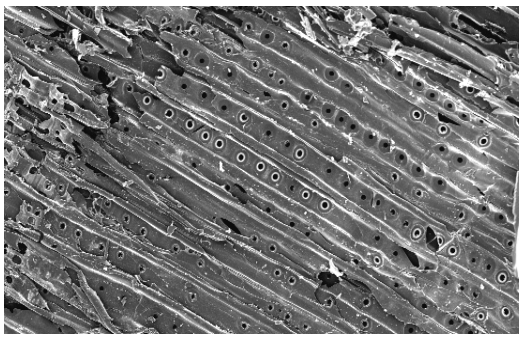

Fig. 2. SEM micrograph of L-AC. Particle size:-1000 +850 µm; Mag.: 500 x 10µm

The mesopore PSD was determined by the Pierce method [13] and results shown in Fig 3, where it was confirmed that the L-AC had uniform mesopores in the narrow range 2.0 – 8.0 nm pore diameter centred at about 2.5 nm pore diameter. From CO_2-adsorption data, the instrument software calculated narrow microporosity distribution (Horvath-Kawazoe method) is shown as insert in Fig. 2. It was observed that the narrow microporosity was mostly 0.4 nm in diameter. However, the measured high N_2-BET surface area (S_{BET}) in Table 1 indicated presence of wide micropore (0.5 – 2.0 nm). Using equation (1), the calculated average pore width (L_{AVE}) of wide micropores available for adsorption was 0.9 nm.

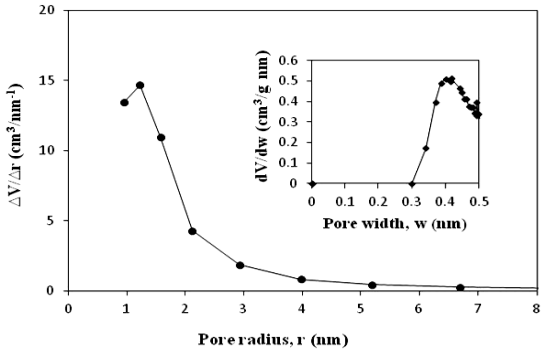

Fig. 3. The mesopore-size distribution (●) of L-AC [Insert: The narrow micropore-size distribution (■) of L-AC]

From Table 1, the L-AC showed high S_{BET} of 1079 m^2/g with wide micropore surface area (S_{MIC}) at ca. 54%, and total pore volume (V_T) of 0.71 cm^3/g with moderate wide micropore volume (V_{MIC}) of 0.25 cm^3/g. The high proportion of mesoporosity (V_T – V_{MIC}) at ca. 65% was important for reduced diffusion limitation of $HCrO_4^-$ oxyanion to interior wide micropores that would be sites of high adsorption potential [13-15]. Reported theoretical calculations have indicated that the important parameter for enhanced adsorption potential in effective micropores is the ratio of micropore size to adsorbate size, with upper ratio limit for primary volume filling in the range 1.5 – 2.0 dependent on actual shape (slit-like or cylindrical) pores [13]. With reference to approximate size of $HCrO_4^-$ (≈ 0.50 nm), narrow micropores (< 0.5 nm) would be closed due to size exclusion effect. Also, the adsorption capacity would be reduced in micropores of same size as $HCrO_4^-$ due to kinetic limitations. Thus, considering the theoretical upper ratio limit of effective micropore size for primary filling at 2.0, it could be assumed that for enhanced adsorption capacity of $HCrO_4^-$ from dilute solutions the effective wide micropore PSD would be in the range 0.50 – 1.0 nm. Thus, the evaluated PSD of L-AC of moderate wide micropore volume of average pore width (L_{AVE} = 0.9 nm) and high proportion of narrow mesoporosity was promising for enhanced capacity and fast kinetics of Cr (VI) oxyanion, subject to enhanced affinity of $HCrO_4^-$ for the in-situ created surface groups.

Table 1. Textural properties of L-AC

S_{BET} (m^2/g)	S_{MIC} (m^2/g)	V_T (cm^3/g)	V_{MIC} (cm^3/g)	L_{AVE} (nm)	D_{ave} (nm)	ρ_b (g/L)
1079	580	0.71	0.25	0.9	2.4	162

D_{ave}: HJB average pore diameter; ρ_b: Bulk density

Fig. 4 shows that the L-AC was highly basic with pH_{PZC} about 10, consistent with the Boehm titration calculations of high total basicity (940 µmol/g) against total acidity (71 µmol/g). The high activation temperature (800°C) basicity of L-AC could be due to presence of thermally stable surface oxygen basic groups (pyrone and chromene) and delocalized π-electrons system on basal graphene layers [26].

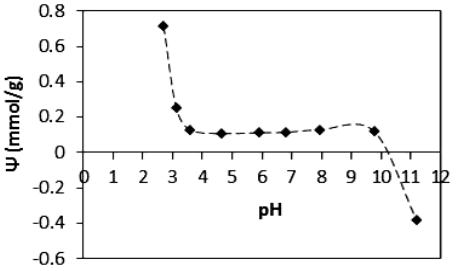

Fig. 4. Proton binding isotherm for L-AC. 298K; < 45 µm

3.2 Effect of pH

The pH influences the ionization of AC surface groups and Cr (VI) in water and, therefore, the evolution of uptake with pH could be used to elucidate the type of surface interactions e.g. complexation or ion exchange or electrostatic attraction or combinations. Fig. 5 shows the effect of pH (2 – 12) on percentage removal of Cr (VI) on L-AC.

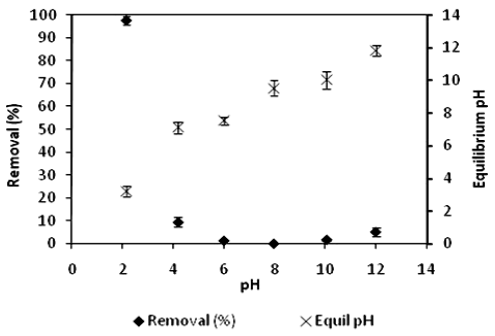

Fig. 5. Effect of pH on sorption of Cr (VI) on L-AC. C_O: 50 mg/l; 298K; -425 + 106 µm: Percentage removal (♦); Equilibrium pH (X)

The results in Fig. 5 showed that percentage removal was high at pH 2 (ca. 98 ± 1.6%) and minimal for pH > 2. A similar trend has been reported [27,28]. On the other hand, the equilibrium pH slightly increased for initial pH (2 – 8), and was similar to initial pH for pH (10 – 12). An only slight increase in equilibrium pH at initial pH 2 suggested that the solution direct reduction of Cr (VI) to Cr (III), catalyzed by surface acidic electron-donor groups and complexation of Cr (III) as suggested in [8,29] may not be the main mechanism of Cr (VI) adsorption. Otherwise, the equilibrium pH would have substantially increased due to consumption of large quantities of solution protons in the reduction process as per equation (18) [17]. The negligible direct reduction of Cr (VI) at pH ≥ 2 has been similarly reported [6,8,17]. For C_O = 100 mg/L, the predominant species is $HCrO_4^-$ in pH 1 – 6.5 [2] and L-AC surface is protonated as shown in Fig. 4. The observed slight increase in equilibrium pH for initial pH < 10 in Fig. 4 may be explained by surface protonation. Significant ion exchange of surface protons for $HCrO_4^-$ at pH 2 as per equation (19) proposed in [6] may also not be the main mechanism, because the L-AC was highly basic with low concentration of acidic groups that would be main sites of ion exchange to account for the measured high ca. 98 ± 1.6% removal for C_O = 100 mg/L at pH 2.

$$HCrO_4^- + 7H^+ + 3e^- \leftrightarrow Cr^{3+} + 4H_2O \quad (18)$$

$$AC\text{-}OH_2^+ + HCrO_4^- \leftrightarrow AC\text{-}OH_2CrO_4^- + H^+ \quad (19)$$

$$AC\text{-}OH_2^+ + HCrO_4^- \leftrightarrow AC\text{-}OH_2^+ (HCrO_4^-) \quad (20)$$

Therefore, the high adsorption at pH 2 was suggestive of primary physical non-specific interactions of electrostatic attraction between $HCrO_4^-$ and protonated surface groups e.g. equation (20). Since the level of acidic groups was low on L-AC, it would be expected that only part of surface bound $HCrO_4^-$ was reduced and complexed. In this study, experiments not shown, the adsorption-coupled reduction and complexation of part of surface bound $HCrO_4^-$ could be supported by loss of Cr (VI) adsorption capacity at ca. 52% on reusability of column regenerated Cr (VI) saturated L-AC bed using 3M NaOH eluent. The observed low adsorption

of chromium oxyanions in pH (2 – 8) in Fig. 5 was attributed to very low level of surface protonation as seen in Fig. 4. While for pH > 10 the L-AC surface was deprotonation and repulsion of chromium oxyanions occurred. Further adsorption tests in this study were conducted at pH 2.

3.3 Adsorption Isotherm and Comparative Cr (VI) Capacities

The equilibrium isotherm data was treated to evaluate the maximum adsorption capacity of L-AC for Cr (VI) from dilute aqueous solution. Generally, for economical and efficient operation of adsorption units, the AC must have high capacity for the solute so that relatively small quantities can be used to effect a given wastewater treatment. Fig. 6 compares the isotherm curves of Cr (VI) on L-AC and commercial AC (Norit RO 0.8). Both ACs exhibited L-type isotherms indicative of weak competition between Cr (VI) and water for active adsorption sites [30]. The isotherm parameters were calculated using the Langmuir (equation (14)) and Freundlich (equation (15)) models and results presented in Table 2.

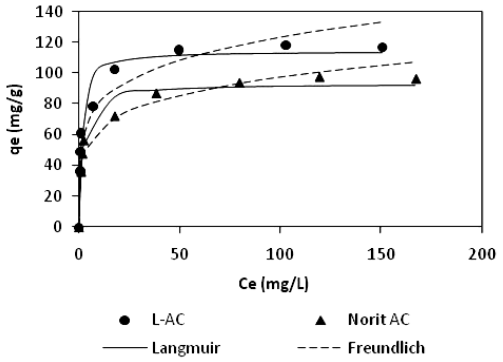

Fig. 6. Adsorption isotherm of Cr (VI) on L-AC and Norit AC (RO 0.8). 298K; pH 2.0 ± 0.3; -200+150 µm: L-AC (●); Norit AC (▲); Langmuir (—); Freundlich(- - -)

According to Table 2, the isotherm data of both ACs were well fitted by the Langmuir model (lowest χ2) that underpins monolayer coverage, suggesting uniform distribution of active adsorption sites [20]. However, L-AC showed high monolayer capacity for Cr (VI) than Norit AC (RO 0.8). A further comparison of Cr (VI) capacities from dilute solutions (< 400 mg/L) in pH 1 - 3 with some literature sawdust low-cost adsorbents/ACs and commercial ACs was summarized in Table 3. It was noticed in Table 3 that the Cr (VI) capacity on sawdust low-cost AC of this study was on the higher side of sawdust low-cost adsorbents/ACs, and competitive with high performance commercial ACs. Due to low-cost, the high Cr (VI) capacity on L-AC would translate into high adsorption capacity per cost of adsorbent compared with expensive commercial ACs [40], and can be used on a once-through basis without considerations for the costly regeneration [32]. This result qualified the L-AC to be very economical and efficient for abatement of Cr (VI) from wastewater, even at large scale. The spent AC would be safely disposed off through a strict toxic sludge containment protocol, otherwise use of the common spent AC incineration method would have a major problem of Cr (VI) thermal decomposition at about 196°C to highly thermal stable and carcinogenic chromium (III) oxide [41].

In majority of studies on adsorption of Cr (VI) on AC the pore structure was not fully characterized. Nevertheless, for dilute solutions, the results in Table 3 indicate that Cr (VI) capacity is not influenced by surface area. Analysis of surface functionality show that low and high Cr (VI) capacities have been obtained on either acidic or basic ACs, suggesting that pore-size distribution (PSD) strongly influences $HCrO_4^-$ capacity on AC. For assumed spherical $HCrO_4^-$ oxyanions (size ≈ 0.5 nm); we calculated the monolayer equivalent surface area (S_{EQ}) of adsorbed $HCrO_4^-$ on L-AC and compared it with the measured wide micropore surface area (S_{MIC}) of L-AC. It was found that S_{EQ} was less than S_{MIC}. With reference to the average wide micropore size available for adsorption (L_{AVE} = 0.9 nm) of L-AC, and the assumed range 0.5 – 1.0 nm (section 3.1) of effective micropore PSD for $HCrO_4^-$ primary volume filling, the calculated $S_{EQ} < S_{MIC}$ showed that only effective micropores with monolayer filling were involved in the adsorption from dilute solution. To support this finding, we treated literature AC characterization results and compared with L-AC. For adequately characterized ACs in Table 3, It was found that always $S_{EQ} < S_{MIC}$, confirming that only an effective microporosity was involved in adsorption from dilute solution, in agreement with results in related study [16]. The high Cr (VI) capacity on the L-AC of this study could be related to presence of large volume of effective micropores with primary filling capacity. It could be argued that the same reason may explain the reported high Cr (VI) capacity on mesoporous silica nanoparticles (SNP) having broad PSD [11]. While the minimal capacity for AC with

L_{AVE} = 0.6 nm (Table 3) could be attributed to almost absence of effective microporosity as confirmed by very large difference between S_{EQ} and S_{MIC}, suggesting that this AC had majority of micropores below 0.6 nm and size exclusion effects could have dominated. On the other hand, for moderate to high V_{MIC} of ACs, the results in Table 3 seem to indicate gradual decrease of capacity with monotonic increase of L_{AVE} above 0.9 nm. The decrease of capacity could be attributed to progressive loss of effective micropores with increase in L_{AVE} > 0.9 nm. The exceptional very low capacity at L_{AVE} = 1.0 nm (Table 3) could be explained in terms of very low V_{MIC}. Interestingly, for ordered mesoporous carbon (OMC) it was observed that S_{EQ} > S_{MIC}: The very high Cr (VI) capacity on OMC of large sized pores may be explained in terms of bilayer or secondary volume filling considering the estimated average pore size available for adsorption (L_{AVE} = 1.7 nm), and high C_O upto 3000 mg/L used in the equilibrium adsorption experiments. The treated results in Table 3 confirm the suggestion that an effective micropore PSD is significant for enhanced sorption capacity of Cr (VI) from dilute aqueous solutions.

3.4 Batch Kinetics and Intraparticle Mass Transfer

Besides high adsorption capacity for Cr (VI), the Cr (VI) uptake rate on L-AC is integral to optimal design of adsorption units for it would affect the throughput. Fig. 7 shows the effect of initial concentration and contact time on sorption of Cr (VI) on L-AC. The L-AC exhibited fast adsorption kinetics that could be associated with the mesostructure that offered reduced diffusion resistance for $HCrO_4^-$ oxyanions to interior wide micropores the sites of high adsorption energy.

Table 2. Isotherm parameters of Cr (VI) on L-AC and Norit AC (RO 0.8) at 298K

Adsorbent	Langmuir constants			Freundlich constants		
	Q_{MAX} (mg/g)	K_L (L/mol)	χ2	K_F (mg/g)	Fr	χ2
L-AC	115	0.83	9.14	52.0	0.18	10.66
Norit AC	94	0.55	3.04	41.0	0.19	4.00

Table 3. Comparison of Cr (VI) capacities from dilute aqueous solutions on low-cost adsorbents and commercial activated carbon at room temperature and pH (1 - 3)

Adsorbent		S_{BET} (m^2/g)	V_{MIC} (cm^3/g)	S_{MIC} (m^2/g)	S_{EQ} (m^2/g)	L_{AVE} (nm)	Q_{MAX} (mg/g)	Ref.
SAC	[A]	0.86	-	-			42.50	[17]
SAC	[A]	1674	-	-			44.05	[28]
SD	[A]	-	-	-			12.78	[31]
CAC		650	-	-			147	[32]
SAC	[A]	-	-	-			22.35	[33]
J. AC	[B]	1305	0.55	-			141	[34]
CAC	[A]	874	0.35	-			132	[34]
P. AC	[A]	751	0.33	-			106	[34]
L. AC	[B]	1459	0.82	1178	339	1.4	84	[35]
LS.AC		1512	0.61	952	142	1.3	35	[1]
L. AC	[B]	1363	0.36	701	376	1.0	93	[35]
P. AC	[B]	86	0.09	180	54	1.0	16	[36]
B. AC		718	0.32	585	360	1.1	89	[37]
CAC		1402	0.46	1370	24	0.6	5.9	[38]
SAC	[B]	1079	0.25	580	465	0.9	115	This study
CAC	[B]	1150	-	-			94	This study
MCS	[A]	4.4	-	-			200	[27]
WB.AC	[B]	-	-	-			59.23	[39]
SNP		760	-	-			111	[11]
OMC		553	0.36	415	764	1.7	189	[12]

SAC: Sawdust activated carbon; SD: sawdust; CAC: commercial activated carbon; J: Jatropha; P: Peanut shell; L: Lignin; LS: Longan seed; B: Bagasse;MCS: Modified corn stalk;WB: Waste bambo; SNP: Silica nanoparticles; OMC: Ordered mesoporous carbon; [A]: Acidic; [B]: Basic; S_{EQ} = monolayer equivalent surface area = (Am Qmax N_A)/M_W; Am: molecular area; N_A: Avogadro constant; M_W: molecular weight; L_{AVE} = 2000v_{mic}/s_{mic}

The applicable rate constant was determined from fitting the pseudo-first order (equation 4.5) and pseudo-second order (equation 4.7) to kinetics data, and results presented in Table 4. The kinetics rate constant is an essential parameter for optimal design of batch adsorption units by use of the contact time model [42]. The results in Table 4 indicated that the pseudo-second order model adequately described the kinetics data (lowest $\chi 2$), as confirmed in Fig. 7. The Pseudo-second model is formulated on chemisorption kinetics [43] and, therefore, its agreement with kinetic data suggested involvement of chemical adsorption, further support of occurrence of some coupled adsorption-reduction of Cr (VI). The analysis of second-order kinetic parameters revealed that the initial adsorption rate, h, increased with an increase in C_O, consistent with results in Fig. 7. On the other hand, the adsorption rate constant, k_2, decreased with an increase in C_O. Similar variation of k_2 with C_O was reported for sorption of Cr (VI) on sawdust [17]. The increase of h with an increase in C_O was attributed to high concentration gradients at high initial concentration causing fast diffusion of $HCrO_4^-$ oxyanion to the AC surface. As would be expected of equilibrium uptake, the q_2 values increased with an increase in C_O. This was attributed to large number of $HCrO_4^-$ oxyanion available for adsorption and hence long equilibrium times as C_O increased.

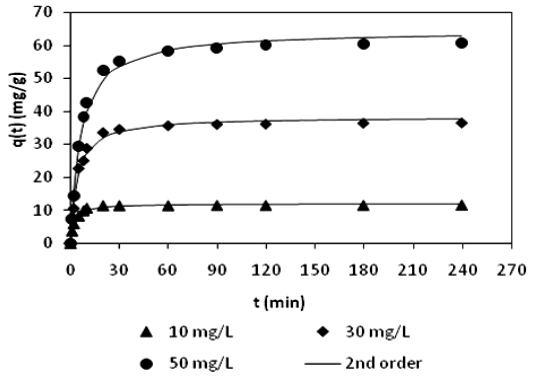

Fig. 7. Effect of initial concentration on batch kinetics for sorption of Cr (VI) on L-AC. 296K; -600+300 µm: 10 mg/L (▲); 30 mg/L (♦); 50 mg/L (●); 2nd order kinetics (—)

The batch diffusion controlling stage was evaluated through calculation of [batch] Biot number (Bi), equation 10. The Biot number is a ratio of mass transfer resistance in the solid phase to mass transfer resistance in the liquid-film round the solid [23,25]. The knowledge of diffusion limiting stage would allow for proper design of process conditions to enhance Cr (VI) uptake. To determine the effective intraparticle diffusion coefficient (D_{eff}), the Patterson model (equations 13 - 17) was fitted to kinetics data and the model performance shown in Fig. 8. While Fig. 9 shows the fitting of the M&W (LDF) rate law (equations 4.12 – 4.14) to kinetic data at C_O = 50 mg/L Cr (VI) in the initial adsorption time < 5 min for determination of the [batch] liquid-film mass transfer coefficient (k_{fb}).

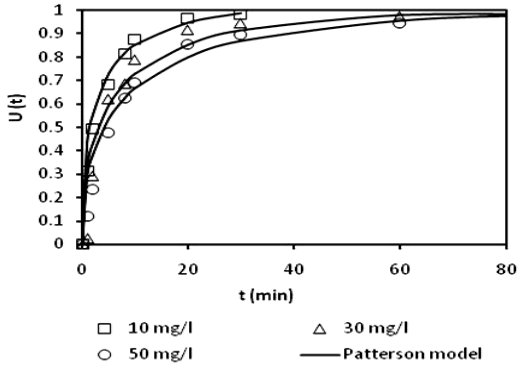

Fig. 8. Fractional attainment to equilibrium for sorption of Cr (VI) on L-AC: 10 mg/L (□); 30 mg/L (∆); 50 mg/L (○); Patterson diffusion model (—)

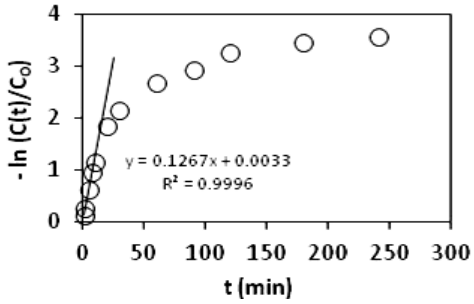

Fig. 9. Application of linear driving force rate law for sorption of Cr (VI) on L-AC. t < 5.0 mins

It can be seen that the Patterson model fit to kinetics data was excellent, with an average error between experimental and model values of ca. ≤ 8% for all concentrations studied. Equally, the M&W (LDF) fit to kinetic data was excellent with the correlation coefficient of R^2 > 0.98 for all concentrations studied. The estimated values of D_{eff} and k_{fb} and Bi are summarized in Table 5. The Patterson model is applicable to intraparticle diffusion control and finite solution case, with

Table 4. Batch kinetics rate parameters for sorption of Cr (VI) on L-AC

Variable	$q_{e(expt)}$ (mg/g)	Pseudo-first order		χ2	Pseudo-second order			χ2
		q_1 (mg/g)	k_1 (/ min)		q_2 (mg/g)	k_2 (g /mg min)	h (mg/ g min)	
C_O (mg/l)					(particle size:-600+300µm; T: 296K)			
10	11.66	11.34	0.35	0.3	12.02	0.0417	6	0.1
30	36.54	35.48	0.19	1.0	38.20	0.0065	9	0.8
50	60.76	58.84	0.13	1.4	61.37	0.0025	10	1.2

Table 5. Estimated diffusion parameters for sorption of Cr (VI) on L-AC

Parameter	w	k_{fb} (x 10^3 cm/s)	D_{eff} (x 10^8 cm^2/s)	Bi
C_O (mg/l)		(Particle size: -600+300µm; T: 296K)		
10	0.977	7.34	6.16	0.96
30	0.971	7.45	3.09	5.15
50	0.961	5.30	2.24	8.18

finite solution case verified by calculated equilibrium partition ratios from equation (17) of 0 < w < 1 for all initial concentrations studied. The magnitudes of estimated D_{eff} (10-8 cm^2/s) and k_{fb} (10-3 cm/s) are typical of metal ions diffusion into AC porous structure reported in literature [23,24] and, therefore, further validating the applicability of the Patterson model and M&W (LDF) rate law to kinetic data. The k_{fb} values were similar at C_O (10 and 30 mg/l), but decreased at C_O = 50 mg/L. Choy et al. [24] have reported a similar trend for sorption of Zn (II) on bone char. The D_{eff} values decreased with an increase in C_O, indicative of increasing intraparticle resistance presumably due to $HCrO_4^-$ anions crowding of the adsorbent surface and, therefore, anions competition for adsorbent pores. Consequently, the *Bi* increased with increase in C_O. Intraparticle diffusion sorely controls the adsorption process for *Bi* > 30, while film diffusion controls the adsorption for *Bi* < 0.5 [23]. Therefore, the calculated (*Bi*) values indicated that intraparticle diffusion resistance was relatively significant for $C_O \geq 20$ mg/L.

4. CONCLUSION

Optimally developed low-cost adsorbent/ activated carbon (AC) of tailored microporosity distribution would provide a sustainable alternative for economical and efficient removal of Cr (VI) from dilute wastewaters. The results of this study showed that adsorbent effective microporosity strongly influences the sorption capacity of Cr (VI) from dilute solutions significant to environmental protection. Consequently, the optimum design of low-cost adsorbent/AC should factor moderate to high micropore volume and effective microporosity of average pore size about 0.9 ± 0.1 nm. Also, a high proportion of mesoporosity is desirable for reduced diffusion limitations to interior effective micropores. The results of this study show that the forward approach of tailoring relevant adsorptive properties at adsorbent preparation stage is important than the backward approach of developing the adsorbent first and then testing for quality. The determining of adsorbent/AC micropore volume and an average effective micropore size from N_2 adsorption isotherm data would be simple routine quality control procedure to ensure quality of developed adsorbent/AC.

ACKNOWLEDGEMENT

The authors gratefully acknowledge the financial support of this project by the National Research Fund of the Tshwane University of Technology, Pretoria, South Africa.

COMPETING INTERESTS

Authors have declared that no competing interests exist.

REFERENCES

1. Jinbei Y, Meiqiong Y, Wentao C. Adsorption of hexavalent chromium from aqueous solution by activated carbon prepared from longan seed: Kinetics, equilibrium and thermodynamics. J. Ind. Eng. Chem. 2015;21:414–422.
2. Mohan D, Pittman CU. Review of activated carbons and low cost adsorbents for remediation of tri- and hexavalent chromium from water. J. Hazard. Mater. 2006;B137:762–811.

3. Ghosh PK. Hexavalent chromium [Cr (VI)] removal by acid modified waste activated carbons. J. Hazard. Mater. 2009;171:116–122.
4. EPA (Environmental Protection Agency), Environmental pollution control alternatives, EPA/625/5-90/025, EPA/625/4-89/023, Cincinnati, US; 1990.
5. Jenkins HDB, Thakur KP. Reappraisal of thermochemical radii for complex ions. J. Chem. Educ. 1979;56(9):576.
6. Liu SX, Chen X, Chen XY, Liu ZF, Wang HL. Activated carbon with excellent chromium (VI) adsorption performance prepared by acid–base surface modification. J. Hazard. Mater. 2007;141: 315–319.
7. Owlad M, Aroua MK, wan Daud WMA. Hexavalent chromium adsorption on impregnated palm shell activated carbon with polyethyleneimine. Bioresour. Technol. 2010;101:5098–5103.
8. Yingxin Z, Wenfang Q, Guanyi C, Min J, Zhenya Z. Behavior of Cr (VI) removal from wastewater by adsorption onto HCL activated Akadama clay. J. Taiwan Inst. Chem. Eng. 2015;50:190–197.
9. Hu J, Chen G, Lo IM. Removal and recovery of Cr (VI) from wastewater by maghemite nanoparticles. Water Res. 2005;39:4528–4536.
10. Zhung-gia N, Jun-wei L, Hanita D, Si-ling N, Mohammed JKB. Reassessment of adsorption–reduction mechanism of hexavalent chromium in attaining practicable mechanistic kinetic model. Process. Saf. Environ. Prot. 2016;102:98–105.
11. Idris SA, Alotaibi KM, Peshkur TA, Anderson P, Morris M, Gibson LT. Adsorption kinetic study: Effect of adsorbent pore size distribution on the rate of Cr (VI) uptake. Microporous Mesoporous Mater. 2013;165:99–105.
12. Chen T, Wang T, Wang DJW, Xue HR, Zhao JQ, Ding XC, Wu SC, He JP. Synthesis of ordered large-pore mesoporous carbon for Cr (VI) adsorption. Mater. Res. Bull. 2011;46:1424–1430.
13. Gregg SJ, Sing KSW. Adsorption, surface area and porosity. 2nd ed. London: Academic Press; 1982.
14. Dabrowski A. Adsorption-from theory to practice. Adv. Colloid Interface Sci. 2001;93:135-224.
15. Marsh H, Rodriguez-Reinoso F. Activated carbon. 1st ed. UK: Elsevier Science & Technology Books; 2006.
16. Centeno TA, Marban G, Fuertes AB. Importance of micropore size distribution on adsorption at low adsorbate concentrations. Carbon. 2003;41:843–846.
17. Gupta S, Babu BV. Removal of toxic metal Cr (VI) from aqueous solutions using sawdust as adsorbent: Equilibrium, kinetics, and regeneration studies. Chem. Eng. J. 2009;150:352–365.
18. Mukosha L, Onyango MS, Ochieng A, Kasaini H. Development of better quality low-cost activated carbon from South African pine tree (*Pinus patula*) sawdust: Characterization and comparative phenol adsorption. Int. J. Chem. Nuclear, Metal. Mater. Eng. 2013;7(7):228-238.
19. Ohkubo T, Iiyama T, Nishikawa K, Suzuki T, Kaneko K. Pore-width-dependent ordering of C_2H_5OH molecules confined in graphitic slit nanospaces. J. Phy. Chem. 1999;B103:1859-1863.
20. Foo KY, Hameed BH. Insight into the modeling of adsorption isotherm systems. Chem. Eng. J. 2010;156:2-10.
21. Mukosha L, Onyango MS, Ochieng A, Taile YL. Sorption characteristics of mixed molecules of glutaraldehyde from water on mesoporous acid-amine modified low-cost activated carbon: Mechanism, isotherm and kinetics. J. Chem. 2014;1-13.
22. Qiu H, Lu LV, Pan BC, Zhang QJ, Zhang WM, Zhang QX. Critical review in adsorption kinetic models. J. Zhejiang Univ. Sci. A. 2009;10(5):716-724.
23. Inglezakis VJ, Poulopoulos SG. Adsorption, ion exchange and catalysis: Design of operations and environmental applications. UK: Elsevier; 2006.
24. Choy KKH, Ko DC, Cheung WC, Porter JF, McKay G. Film and intraparticle mass transfer during the adsorption of metal ions onto bone char. J. Colloid Interface Sci. 2004;271:284-295.
25. Cooney DO. Adsorption design for wastewater. USA: CRC Press; 1999.
26. Villacanas F, Pereira MFR, Orfao JJM, Figueiredo JL. Adsorption of simple aromatic compounds on activated carbons. J. Colloid Interface Sci. 2006;293:128–136.
27. Suhong C, Qinyan Y, Baoyu G, Qian I, Xing X. Removal of Cr (VI) from aqueous

solution using modified corn stalks: Characteristic, equilibrium, kinetic and thermodynamic study. Chem. Eng. J. 2011;168:909–917.
28. Karthikeyan T, Rajgopal S, Miranda LR. Chromium (VI) adsorption from aqueous solution by *Hevea brasilinesis* sawdust activated carbon. J. Hazard. Mater. 2005;B124:192–199.
29. Hu J, Chen C, Zhu X, Wang X. Removal of chromium from aqueous solution by using oxidized multiwalled carbon nanotubes. J. Hazard. Mater. 2009;162:1542–1550.
30. Dabrowski A, Podkoscielny P, Hubicki ZM. Adsorption of phenolic compounds by activated carbon – a critical review. Chemosphere. 2005;58:1049–70.
31. Kapur M, Mondal MK. Mass transfer and related phenomena for Cr (VI) adsorption from aqueous solutions onto *Mangifera indica* sawdust. Chem. Eng. J. 2013;218: 138–146.
32. Aksu Z, Gonen F, Demircan Z. Biosorption of chromium (VI) ions by Mowital®B30H resin immobilized activated sludge in a packed bed: Comparison with granular activated carbon. Process Biochem. 2002;38:175–186.
33. Politi D, Sidiras D. Wastewater treatment for dyes and heavy metals using modified pine sawdust as adsorbent. Procedia Eng. 2012;42:1969–1982.
34. Gueye M, Richardson Y, Kafack TF, Blin J. High efficiency activated carbons from African biomass residues for the removal of chromium (VI) from wastewater. J. Environ. Chem. Eng. 2014;2:273–281.
35. Gonzalez-Serrano E, Cordero T, Rodriguez-Mirasol J, Cotoruelo L, Rodriguez JJ. Removal of water pollutants with activated carbons prepared from H3PO4 activation of lignin from kraft black liquors. Water Res. 2004;38:3043–3050.
36. AL-Othman ZA, Ali R, Naushad MU. Hexavalent chromium removal from aqueous medium by activated carbon prepared from peanut shell: Adsorption kinetics, equilibrium and thermodynamic studies. Chem. Eng. J. 2012;184:238–247.
37. Demiral H, Demiral I, Tumsek F, Karabacakoglu B. Adsorption of chromium (VI) from aqueous solution by activated carbon derived from olive bagasse and applicability of different adsorption models. Chem. Eng. J. 2008;144:188–196.
38. Gottipati R, Mishra S. Simultaneous removal of trivalent and hexavalent chromium by activated carbon: Effect of solution pH and pore size distribution of adsorbent. Environ Prog Sustain Energy. 2013;32(4):1030-1035.
39. Tamirat D, Khalid S, Shimeles AK. Adsorption of hexavalent chromium from aqueous solution using chemically activated carbon prepared from locally available waste of bamboo (*Oxytenanthera abyssinica*). Environ. Chem. 2014;1-9.
40. Argun EM, Dursun S, Ozdemir C, Karatas M, Heavy metal adsorption by modified oak sawdust: Thermodynamics and kinetics. J. Hazard. Mater. 2007;141:77–85.
41. Guertin J, Jacobs JA, Avakian CP. Chromium (VI) handbook. UK: CRC Press; 2004.
42. Ho SY, McKay G. A two-stage batch sorption optimized design for dye removal to minimize contact time. Trans. Icheme. Part B. 1998;76:313–318.
43. Ho YS, McKay G. Pseudo-second order model for sorption processes. Process Biochem. 1999;34:451-465.

Peer-review history:
The peer review history for this paper can be accessed here:
http://sciencedomain.org/review-history/19612